THE JOURNAL OF PHYSICAL CHEMISTRY B

Article

Cite This: J. Phys. Chem. B 2018, 122, 5797−5808

pubs.acs.org/JPCB

Formation of Catalytically Active Binuclear Center of Glycerophosphodiesterase: A Molecular Dynamics Study

Thomas J. Paul,[†] Gerhard Schenk,[‡] and Rajeev Prabhakar*[,†]

[†]Department of Chemistry, University of Miami, Coral Gables, Florida 33146, United States

[‡]School of Chemistry and Molecular Biosciences, The University of Queensland, St. Lucia, Queensland 4072, Australia

Supporting Information

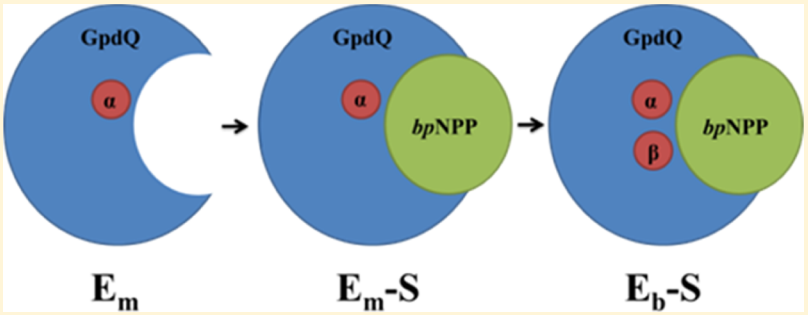

ABSTRACT: Glycerophosphodiesterase (GpdQ) is a binuclear metallophosphatase that catalyzes the hydrolytic cleavage of mono-, di-, and triphosphoester bonds of a wide range of critical molecules. Upon substrate binding, this enzyme undergoes a complex transformation from an inactive mononuclear form ($\mathbf{E_m}$, where the metal resides in the α site) to an active binuclear center ($\mathbf{E_b}$-**S**, with metals bound to both the α and β sites) through a mononuclear, substrate-bound intermediate state ($\mathbf{E_m}$-**S**). In this study, all-atom molecular dynamics simulations have been employed to investigate structures and dynamical transformations in this process using eight different variants, i.e., five wild-type and three mutant forms of the enzyme. Additionally, the effects of an actual substrate, bis-(*para*-nitrophenyl) phosphate (b*p*NPP), a metal-bridging nucleophilic hydroxyl, and specific first and second coordination shell residues have been investigated. The initial binding of the substrate to $\mathbf{E_m}$ enhances the metal binding affinity of the α site and prepares the β site for coordination of the second metal ion. These results are in agreement with stopped-flow fluorescence and calorimetry data. In $\mathbf{E_b}$-**S**, the computed increase in the substrate and metal (both α and β) binding energies is also in line with the experimental data. However, removal of the substrate from this complex is found to cause substantial reduction in binding energies of both α and β metals. The role of the substrate in the creation and stabilization of the active site predicted in this study is supported by the kinetic measurements using both stopped-flow and nuclear magnetic resonance techniques. Importantly, residue Asn80, a ligand of the metal in the β site, exhibits coordination flexibility by acting as a gate in the formation of $\mathbf{E_b}$-**S**, in good agreement with mutagenesis and spectroscopic data.

1. INTRODUCTION

Binuclear metallophosphatases are ubiquitous in bacteria, yeast, plants, and mammalian organisms.[1−4] These enzymes have been implicated in a wide range of critical chemical/biochemical processes such as iron transport,[1] generation of reactive oxygen species,[2,3] DNA replication, and bone turnover.[4] They catalyze the hydrolytic cleavage of phosphoester bonds of a variety of biological substrates.[5−9] There are three types of phosphoester bonds (mono-, di-, and triesters) that are cleaved by specialized enzymes known as phosphomono-, phosphodi-, and phosphotriesterases, respectively. However, glycerophosphodiesterase (GpdQ) from *Enterobacter aerogenes*, while nominally a diesterase, is highly promiscuous, degrading substrates representing each of the three phosphate esters over a large pH range.[10−12] Additionally, this enzyme possesses the ability to degrade synthetic organophosphates and phosphorothiolates and thus may be used as a catalyst to remediate pesticide-polluted environments and deactivate highly toxic nerve agents (e.g., sarin).[13−17] The crystal structures of Co^{2+}- and Fe^{2+}-substituted GpdQs have been resolved at 1.9 Å (PDB ID: 3D03) and 2.2 Å (PDB ID: 2ZO9) resolution, respectively,[18] and demonstrate that this enzyme is structurally similar to other α/β sandwich binuclear phosphoesterases such as purple acid phosphatases (PAPs)[19−25] and Mre11 nuclease.[26] Furthermore, its active site is analogous to that of other binuclear metallohydrolases such as methionine aminopeptidase,[9,27] metallo-β-lactamases,[8,28] and, in particular, the cyclic phosphodiesterase Rv0805[29] from *Mycobacterium tuberculosis*, whose seven metal-coordinating amino acid ligands are identical to those of GpdQ (Figure 1). The catalytic center provides two binding sites for metal ions, designated as α and β sites. Each metal ion is coordinating to four amino acid

Received: February 28, 2018
Revised: April 10, 2018
Published: May 3, 2018

DOI: 10.1021/acs.jpcb.8b02046
J. Phys. Chem. B 2018, 122, 5797−5808

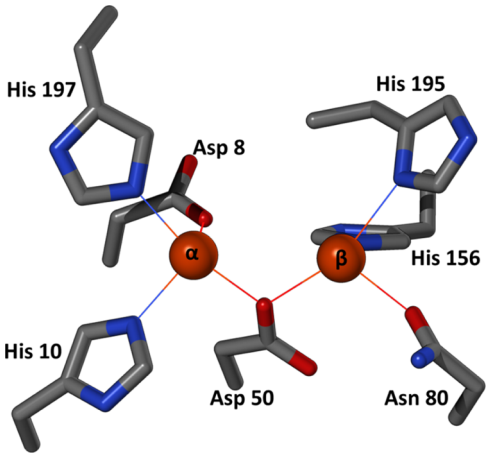

Figure 1. X-ray structure of the active site of GpdQ.

residues;[18] the one in the α site interacts with Asp8, His10, and His197, whereas the one in the β site coordinates to His156, His195, and Asn80. Asp50 is a bridging residue that connects both metal centers.

The metal ion compositions of binuclear metallohydrolases include homonuclear (i.e., Zn−Zn, Mn−Mn, Ni−Ni, etc.) and heteronuclear (Fe−Zn, Mn−Ni, etc.) combinations.[5,7] Anomalous scattering experiments have indicated that Fe(II) is likely to be the preferred metal ion in the more buried α site.[13] However, the preferred metal ion composition of the active in vivo enzyme remains obscure, especially because metal substitution experiments have demonstrated that a range of divalent metal ions such as Zn(II), Cd(II), Mn(II), and Co(II) can reconstitute catalytic activity.[12,18,30,31] Independent of the metal composition, various spectroscopic and thermodynamic methods [X-ray absorption and diffraction, electron paramagnetic resonance, and isothermal titration calorimetry (ITC)] indicate that the α site possesses a higher metal binding affinity than the β site.[10,13,30,32] Indeed, in the absence of a substrate molecule, the enzyme is in a catalytically inactive monometallic state ($\mathbf{E_m}$) and only in the presence of a substrate molecule (or a substrate mimic), a catalytically active bimetallic active center is formed.[13,21] The substrate has been proposed to prepare ("prime") the active site for binding of the second metal to the β site.[13] A combination of structural, spectroscopic, and kinetic data collected for the Co(II) derivative of GpdQ suggests that the substrate-induced activation of the enzyme progresses via three distinct stages (Figure 2).[13,21] In the first stage (characterized by $\mathbf{E_m}$), in the absence of the substrate, only the α site is occupied by a metal. In the next step, in a virtually irreversible process, rapid substrate binding in the vicinity of the α site and subsequent conformational changes create the mononuclear $\mathbf{E_m}$-**S** complex. In $\mathbf{E_m}$-**S**, the β site is primed for metal binding. In the third and final step, a metal binds to the β site and the catalytically active binuclear complex ($\mathbf{E_b}$-**S**) is generated in a relatively fast process (rate = ∼40 s^{-1}).[13] It is noteworthy that this species has been postulated to assemble only in the presence of the substrate or substrate analogues.[13] Three amino acid residues, one in the first coordination shell (Asn80) and two in the second (His81 and His217), have been proposed to play important roles in the creation of $\mathbf{E_b}$-**S**. On the basis of magnetic circular dichroism spectroscopy, Asn80 has been implicated in binding both the substrate and metal in the β site.[13] However, the initial coordination between this residue and the metal in the β site is gradually (over ∼1 min) disrupted as the substrate is reoriented to form the optimal conformation. These structural modifications are likely to be facilitated by the hydrogen bond network that links Asn80 to the substrate binding site and also includes the second coordination shell residues His81 and His217 that facilitate both the positioning of the substrate and the coordination of the metal ion in the β site. The substitution of Asn80 with the nonpolar Ala (Asn80Ala mutant) has been reported to increase the catalytic activity, while decreasing the binding affinities of both the substrate and the metal in the β site.[18] However, its mutation to a negatively charged Asp residue (Asn80Asp mutant) leads to a mutant with greatly reduced reactivity because of the loss of coordination flexibility associated with the tight binding of the Asp residue to the metal in the β site.[33] In contrast, the substitutions of His217 and

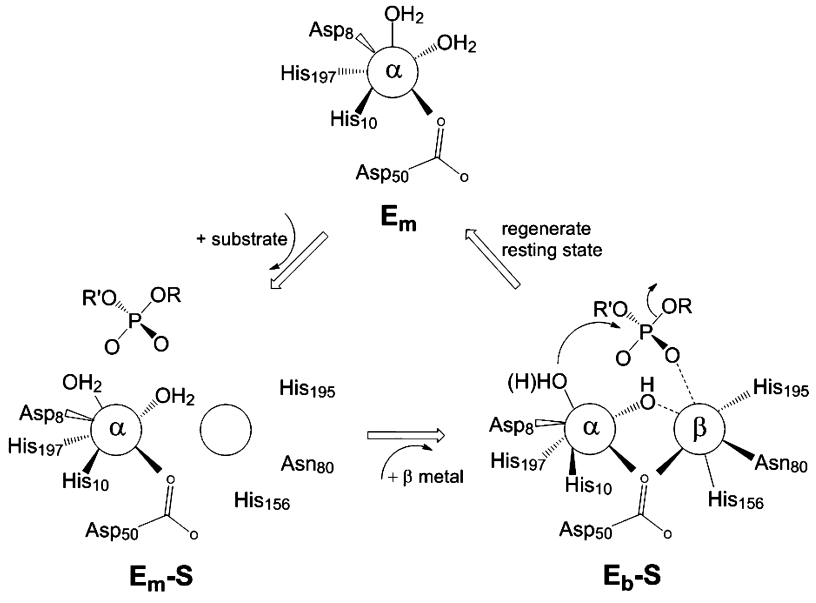

Figure 2. Proposed mechanism for the generation of the active binuclear $\mathbf{E_b}$-**S** species based on extensive experimental data.[13]

DOI: 10.1021/acs.jpcb.8b02046
J. Phys. Chem. B 2018, 122, 5797−5808

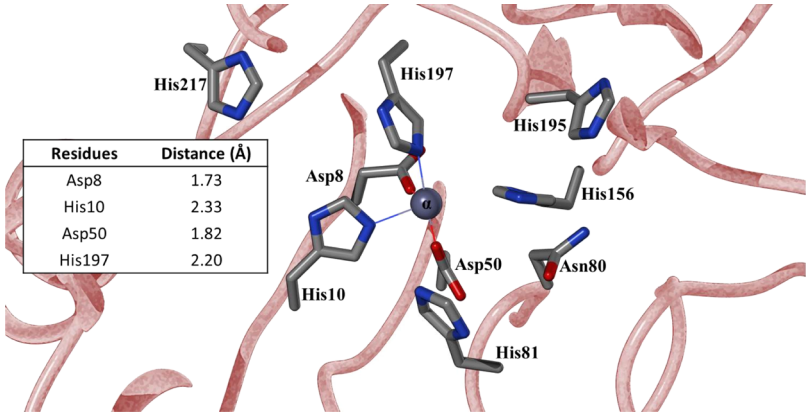

Figure 3. Most representative structure of the mononuclear form ($\mathbf{E_m}$) of GpdQ from MD simulations. The (α) metal is shown in purple and coordinating distances are shown in the table.

His81 by alanine have little effect on the reactivity of the enzyme but enhance the affinity of the metal in the β site.[13] The association between substrate binding, coordination flexibility, and reactivity has not previously been observed for binuclear hydrolases and is in stark contrast to the enzyme Rv0805 where, despite identical metal ligands, the coordination numbers of the metals in the active site are not affected by substrate binding.[29] However, a similar connection between coordination flexibility and substrate binding has also been observed for soy bean lipoxygenase,[34,35] and this relationship is likely to be prevalent in other enzymes as well.

Currently, the only available structures of GpdQ contain a bimetallic center and were obtained from crystals that were grown either in the presence of excess metal ions and/or the substrate mimic and product phosphate. Consequently, the precise mechanism of how substrate binding first primes the active site to accommodate a second metal ion (thus converting $\mathbf{E_m}$-**S** to $\mathbf{E_b}$-**S**) and then activates a metal-bridging hydroxyl ion for a nucleophilic attack on that substrate while altering the coordination number of the metal in the β site is not known. All-atom molecular dynamics (MD) simulations provide an ideal approach to investigate these aspects of this complex reaction mechanism. Our results will provide atomistic level understanding of the functioning of this important enzyme.

2. COMPUTATIONAL DETAILS

The 1.9 Å structure of the Co(II) derivative of GpdQ (PDB ID: 3D03) was used as a starting point for the computational analysis of the reaction mechanism.[18] The bis-(*para*-nitrophenyl) phosphate (b*p*NPP)-bound enzyme−substrate complex was optimized without any geometrical constraint at the B3LYP[36]/6-31G(d)[37] level using the Gaussian 09[38] program package. Additionally, restrained electrostatic potential charges were calculated and used to form a topology file using an antechamber,[39,40] an in-built tool in AMBER.[41] Molecular docking procedures were performed using AutoDock Vina 1.5.6 software[42] to explore the binding of b*p*NPP to GpdQ and generate the starting structure for MD simulations.[42] The size of the grid was chosen to cover the entire active site of GpdQ, with a spacing of 1.00 Å. Using an exhaustiveness value equal to 20, the docking trails yielded 20 poses for each system. The following three separate substrate binding motifs were used for the docking: (1) singly coordinated to the α metal, (2) singly coordinated to the β metal, and (3) doubly coordinated (bridging) to both metals (as shown in the crystal structure). In the subsequent MD simulations using these poses, the substrate was found to shift from a singly coordinated form to the bridging conformation. Furthermore, the initial structures of all three stages of the catalytic cycle were constructed using the crystal structure (3D03), where the bound substrate mimic/product phosphate and Co(II) ions were replaced with b*p*NPP and Zn, respectively. Zn^{2+} and Co^{2+} are chemically quite similar. However, because of the redox stable +2 oxidation state of the Zn ion, more accurate force field parameters for this metal are available. Additionally, the metal ion does not play a direct role in dynamical transformations investigated in this study. The MD simulations of $\mathbf{E_m}$, $\mathbf{E_m}$-**S**, and $\mathbf{E_b}$-**S** were performed using the GROMACS program,[43,44] utilizing the AMBER03[45] force field. This classical force field does not include polarization and charge-transfer effects. However, these effects are expected to exhibit only minor effects on the MD equilibrated structures. For all simulations, a cubic box was used with dimensions of 70 × 90 × 70 Å. These dimensions were selected to minimize the adverse effects that could result from the applied periodic boundary conditions. TIP3P[46] water molecules were used to saturate the box. Some of the water molecules used were substituted by sodium and chloride ions to simulate a physiological ion concentration (154 mM) and neutralize the system's overall charge (−11). The simulations were performed utilizing a two-step approach. First, the MD structures were energy-minimized, utilizing a steepest descent method freezing active site to minimize rearrangement. Second, these minimized structures were used as the starting point for the MD simulations. In the first step, 30 ns simulations were run, where the active site contact atoms (atoms in close proximity to the Zn ions) were constrained and overall active site conformations maintained. In the second step, the active site constraints were removed and 100 ns production runs on each system (more than 1 μs in total) performed. The simulations were performed using a constant number of particles (N), pressure (P), and temperature (T) which has been termed the *NPT* ensemble. The LINCS algorithm[47] was used to constrain the bond lengths within the peptide, whereas the SETTLE algorithm[48] was used to constrain the water molecules. A particle mesh Ewald method[49] was used to calculate the long-range electrostatic interactions. Trajectories were computed at a time step of 2 fs where data were saved every 500 steps. Normal ionization states at pH 7.0 were used for all amino acid residues. The MD trajectories were analyzed using the inbuilt tools within GROMACS. We used the most

DOI: 10.1021/acs.jpcb.8b02046
J. Phys. Chem. B 2018, 122, 5797−5808

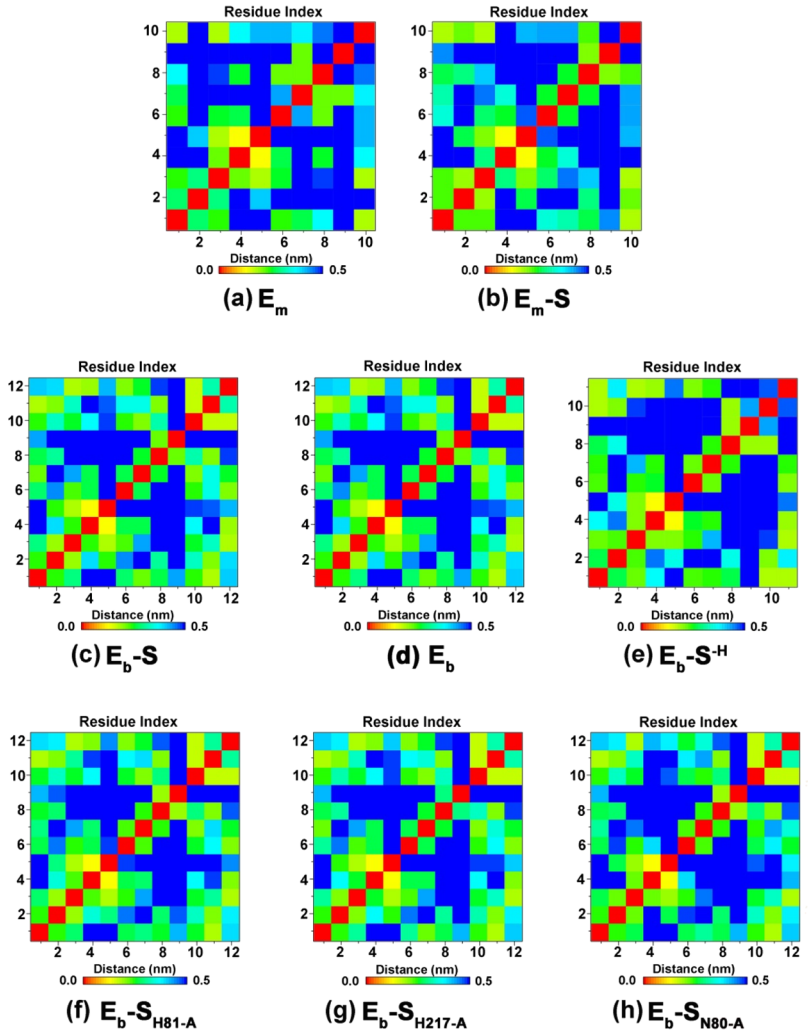

Figure 4. Contact maps of all complexes showing only the active site and secondary shell residues. Color scale bars have been used at a range of 0−0.5 nm.

representative structures for the structural elucidation, which were derived from a cluster analysis on the basis of their occurring frequency, with a strict root-mean-square deviation (rmsd) cutoff of 0.30 nm. Binding energies were calculated for the substrate−protein complex, as well as for both active site metals. These calculations were carried out on the most representative structures taken from cluster analysis utilizing the molecular mechanics Poisson−Boltzmann surface area method,[50,51] which was combined with MD simulations to incorporate both fluctuations and entropic contributions to the binding energy.[51,52] The energy components E_{MM}, G_{polar}, and $G_{nonpolar}$ of each complex were determined for 10 snapshots along the production trajectories at 10 ns intervals. The E_{MM} energies were calculated using Lennard-Jones and Coulomb potentials as implemented in the AMBER force field. The G_{polar} energetic component was calculated by generating a box using the outermost coordinates of each molecular system in each dimension. The box was expanded by 1.5 times to obtain a coarse grid box, whereas a finer grid box extending 5 Å was used. Radii of 0.95 and 1.81 Å were used for the sodium and chloride ions, respectively, with an ionic strength of 0.150 M. The values of the vacuum and solvent dielectric constants were 1 and 80, respectively, whereas a value of 2 was used for the protein dielectric, which is typical for considering only electronic polarization within the protein. Additionally, a van der Waals radius of 2.1 Å was used to describe the zinc metal centers (α- and β-sites). Contact maps and secondary structure diagrams were generated for all complexes studied from production runs utilizing the inbuilt tools mdmat and DSSP,[53,54] respectively, within the GROMACS package. For the contact maps, the active site residues (primary and secondary shell) and metal centers were chosen as reference to highlight slight differences in their overall conformations. The active site residues are labeled in numerical order; for example, residue 1 from Figure 3 is Asp8, residue 2 is His10, and so forth. YASARA,[55,56] Chimera,[57] and photoshop programs were used for visualization and for the preparation of the structural diagrams presented in this study.

3. RESULTS AND DISCUSSION

In this study, all-atom unrestrained MD simulations in aqueous solution were performed on eight different structures, five wild-type (wt) and three mutant forms (Asn80Ala, His81Ala, and His217Ala), representing three mechanistic stages of the catalytic cycle employed by GpdQ. The substrate b*p*NPP was included in the structures of both wt and three mutant forms of this enzyme. The binding of b*p*NPP within the active site caused significant conformational changes only in the first and

DOI: 10.1021/acs.jpcb.8b02046
J. Phys. Chem. B 2018, 122, 5797−5808

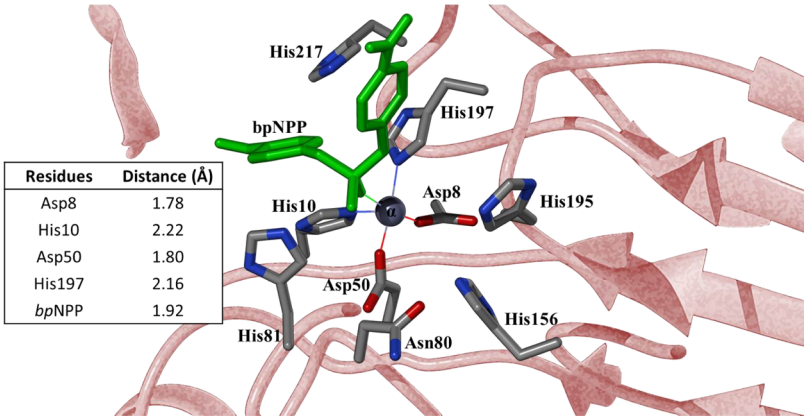

Figure 5. Most representative structure of the mononuclear substrate-bound form ($\mathbf{E_m}$-**S**) of GpdQ from MD simulations. The (α) metal is shown in purple, whereas the substrate b*p*NPP in green. The coordinating distances are provided in the table.

second coordination shell residues, but the overall structure of GpdQ remained unchanged. The computed rmsd values indicated that the equilibration of all of these structures requires at least 30 ns of simulation time. In the thermodynamically equilibrated regions, no trajectory exhibited significant changes and the overall rmsd value remained below 0.8 nm (Figures S1 and S2).

3.1. Structure of the Mononuclear ($\mathbf{E_m}$) Complex. The mononuclear structure ($\mathbf{E_m}$) represents the inactive state of GpdQ. In $\mathbf{E_m}$, only the α metal site is occupied and the substrate is not present at the active site. In this state, the metal ion is directly coordinated to Asp8, His10, Asp50, and His197. The remaining vacant sites may be occupied by one or two solvent water molecules (Figure 2). The starting structure of this species for MD simulations was obtained by removing both the substrate and the metal in the β site from the X-ray structure of GpdQ (PDB ID: 3D03).[18] The most representative structure derived from this simulation is shown in Figure 3. In this structure, all of the first shell residues (Asp8, His10, Asp50, and His197) remained coordinated to the metal in the α site at distances of 1.73, 2.33, 1.82, and 2.20 Å, respectively. Additionally, two water molecules interacted with this metal ion but are not shown. In $\mathbf{E_m}$, the largest fluctuations were observed within Asp50 that shifted and associated with the metal in the α site. This is not surprising as there is no metal present in the β site to interact with this residue. In this structure, another flexible first shell residue, Asn80, remains exposed to the solvent in what looks like an open conformation (Figure 3). The flexible nature of Asn80 is not unexpected because experimental data (vide supra) have demonstrated that it is a key residue for the binding of the metal in the β site to form the enzyme–substrate complex.[13,18] The second coordination shell residues His81 and His217 that facilitate the positioning of the substrate and the coordination of the metal in the β site through an extensive hydrogen bond network surround the metal in the α site in this resting state structure. The contact maps show that His81 is positioned closer to the metal in the α site (~4.5 Å) than His217 (≥5.0 Å; Figure 4a). Embedded into this hydrogen bond network are also residues Tyr19 and Asn53 (not shown in Figure 3), which have been proposed to play a major role in substrate binding and catalysis.[18] Last, together with Asp50 and Asn80, His156 and His195 define the β metal site in a rather open conformation.

3.2. Structure of the Substrate-Bound Mononuclear ($\mathbf{E_m}$-S) Complex. The binding of the substrate b*p*NPP to the $\mathbf{E_m}$ species generates a mononuclear enzyme–substrate ($\mathbf{E_m}$-**S**) complex. The most representative structure obtained from MD simulation shows that b*p*NPP replaces a water molecule that bound to the metal in the α site in $\mathbf{E_m}$ (Figure 5). The substrate monodentately coordinates to the metal in the α site at a distance of 1.92 Å. Binding energy calculations indicate the formation of a stable complex with a free-energy change of −13.9 kcal/mol (Table 1). Amino acids (Asp8, His10, Asp50, and His197) and one water ligand remained bound to the metal ion and complete the first coordination shell. However, there are some conformational changes observed in the active site because of the binding of the substrate. In comparison to $\mathbf{E_m}$, the four amino acid ligands in $\mathbf{E_m}$-**S** are bound more strongly to the metal in the α site, evidenced through shorter bond distances (Figure 5). Indeed, binding energy calculations indicate strong binding of the metal to the α site (−93.0 kcal/mol). In particular, the bond distance involving His10 has decreased substantially (by 0.11 Å) as the substrate exerts a slight crowding effect on the active site [residue index (RI) (2,10) transition from dark blue to light green in Figure 4b]. The enhanced metal affinity of the substrate-bound complex is in agreement with a recent ITC study that demonstrated a considerable reduction in the K_d value of the metal upon the addition of the reactant.[32]

Table 1. Binding Energies of the Substrate b*p*NPP Obtained from MD Production Trajectories[a]

complex	ΔE_{vdW}	ΔE_{elec}	ΔG_{polar}	$\Delta G_{nonpolar}$	$\Delta G_{binding}$
$\mathbf{E_m}$-**S**	−11.9	−30.5	30.7	−2.2	−13.9 ± 8.0
$\mathbf{E_b}$-**S**	2.9	−81.9	48.8	−1.7	−31.9 ± 5.2
$\mathbf{E_b}$-$\mathbf{S^{-H}}$	−5.3	−116.1	71.0	−2.1	−52.6 ± 7.1
$\mathbf{E_b}$-$\mathbf{S_{H81\text{-}A}}$	6.2	−88.7	50.8	−1.5	−33.2 ± 4.5
$\mathbf{E_b}$-$\mathbf{S_{H217\text{-}A}}$	3.8	−87.1	49.8	−1.5	−35.0 ± 4.1
$\mathbf{E_b}$-$\mathbf{S_{N80\text{-}A}}$	3.4	−92.9	62.8	−1.6	−28.3 ± 3.5

[a]The energies are in kilocalories per mole.

Another significant change upon substrate binding is apparent in the position of residue Asn80, which is shifted further away from the metal in the α site by roughly ~1.0 Å; its side chain rotates to accommodate the binding of a metal to the β site [RI (4,10) in Figure 4b]. However, was significantly lower than the fully active and mutant forms of GpdQ.

The key second coordination shell residues, His81 and His217, condense around the metal-bound substrate molecule.

DOI: 10.1021/acs.jpcb.8b02046
J. Phys. Chem. B 2018, 122, 5797–5808

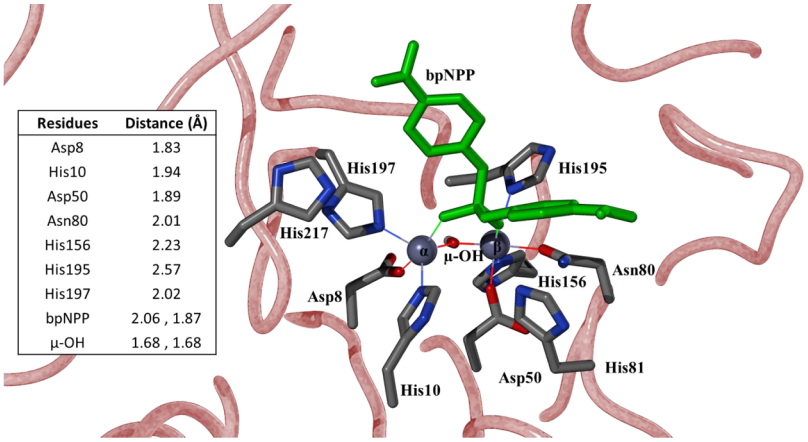

Residues	Distance (Å)
Asp8	1.83
His10	1.94
Asp50	1.89
Asn80	2.01
His156	2.23
His195	2.57
His197	2.02
bpNPP	2.06 , 1.87
μ-OH	1.68 , 1.68

Figure 6. Most representative structure of the active binuclear substrate-bound form ($\mathbf{E_b}$-**S**) of GpdQ from MD simulations. The (α) and (β) metals are shown in purple, whereas the substrate b*p*NPP is in green. The coordinating distances are provided in the table.

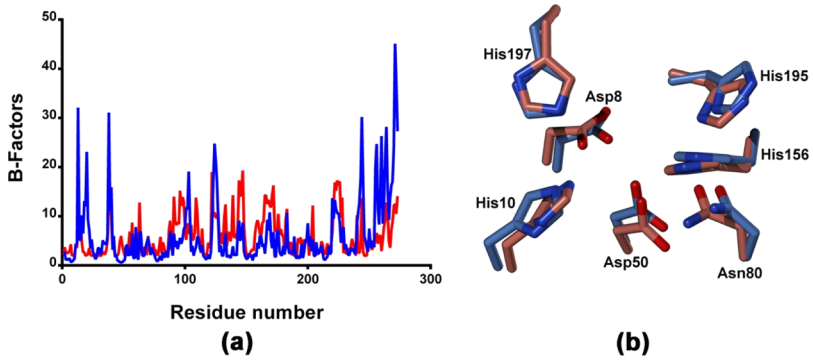

Figure 7. (a) Comparison between the measured (red) and computed (blue) *B*-factors. Computed *B*-factors have been scaled by a factor of 8 for easier comparison. (b) Superposition of the structure of the binuclear metal center $\mathbf{E_b}$-**S** (light pink carbons) derived from MD simulations with the corresponding X-ray structure (light blue carbons).

They form weak interactions (CH−Π and Π−Π) with the aromatic ring of the substrate and thus stabilize its position within the active site (Figure 5). Arg12 (not shown) also provides a further stabilization of the substrate's position through a hydrogen bond (2.91 Å) between its terminal guanidinium group and the nitro group of b*p*NPP. Additionally, in comparison to the substrate-free mononuclear enzyme residue, His195 is rotated closer to Asn80, thus preforming ("priming") a binding pocket for the second metal ion [RI (7,4) transition from light blue to a dark green color in Figure 4b].

In summary, in this initial phase of the reaction cycle, substrate binding enhances the metal affinity of the α site by 20.0 kcal/mol, while priming the β site for binding of the second metal ion. This is in good agreement with stopped-flow fluorescence data that demonstrated that in a rapid initial phase of the catalytic cycle ($k_{obs} \approx 350\ s^{-1}$), a "primed" $\mathbf{E_m}$-**S** complex is formed that has enhanced metal affinity.[13] Indeed, using calorimetry, an enhancement of the metal affinity in the presence of a substrate mimic could be demonstrated.[32]

3.3. Structure of the Catalytic Binuclear ($\mathbf{E_b}$-S) Complex. In the third stage of the catalytic cycle, the binding of a metal ion to the β site in $\mathbf{E_m}$-**S** ($k_{obs} \approx 40\ s^{-1}$)[13] generates a catalytically active binuclear complex ($\mathbf{E_b}$-**S**). The most representative structure of $\mathbf{E_b}$-**S** derived from MD simulation indicates that the binuclear core [(Asp8, His10, His197)(α)−(β)(Asp50, Asn80, His156, His195)] of this complex is held together by a bridging hydroxyl ion and the substrate, which forms a μ-1,3 bidentate complex with the metals (Figure 6). The *B*-factors of the C^{α} atoms calculated from the root-mean-square-fluctuation (rmsf) are in excellent agreement with the crystallographic factors of the X-ray structure (PDB ID: 3D03; Figure 7a). Furthermore, the rmsd value calculated from the superposition of the crystallographic and simulated active site structures of $\mathbf{E_b}$-**S** is only 0.42 Å (Figure 7b), validating the accuracy of the MD simulations. In both structures, all first coordination shell residues lie within bond-forming distances of the metals and the bridging hydroxyl group is positioned opposite to the substrate. However, the metal−metal distance (3.13 Å) in the equilibrated structure is 0.56 Å shorter than the one observed in the crystal structure, which may be partially due to the difference in the identity of the substrate (b*p*NPP vs PO_4).[18] On the basis of bond length, the interaction of b*p*NPP is stronger with the metal in the β site than the one in the α site (1.87 Å vs 2.06 Å, respectively; Figure 6). The coordination numbers of the metals in the α and β sites are five and six, respectively (Figure 6). Among the first coordination shell residues, His195 is the weakest ligand (bond distance = 2.57 Å). It appears that Asn80 acts initially as a strong ligand for the metal in the β site (bond distance = 2.01 Å), thereby stabilizing the active site. Additionally, this residue's backbone carbonyl oxygen atom interacts with the side chain of Asp50 through a strong hydrogen bond at a distance of 1.91 Å. This hydrogen-bonding interaction was also observed in the crystal structure of GpdQ. During the transition from $\mathbf{E_m}$-**S** to $\mathbf{E_b}$-**S**, Asp50 switched its position so that it interacts predominantly with the

DOI: 10.1021/acs.jpcb.8b02046
J. Phys. Chem. B 2018, 122, 5797−5808

metal in the β site (the M_α−O_{Asp50} and M_β−O_{Asp50} distances are 3.22 and 1.89 Å, respectively). In contrast, in the crystal structure, this residue is bridging both metal ions. Again this variation may be due, at least partially, to the use of an actual substrate (b*p*NPP) in the MD simulations, contrasting the use of the smaller phosphate molecule in the crystallographic (and spectroscopic) studies.

Similar to the **E_m-S** complex, the second coordination shell residue His81 stabilizes the substrate at the active site through a CH−Π interaction (at a distance of 2.91 Å) but the previously observed interaction between His217 and the substrate is lost in the bimetallic complex. This loss is compensated by (i) a strong hydrogen bond between the α-amino group of Gln166 and the nitro group of the substrate (2.18 Å) and (ii) a CH−Π interaction between the terminal methyl group of Met167 and the aromatic ring of b*p*NPP (2.71 Å). Additionally, His81 rotated to increase its interactions with the aromatic rings of b*p*NPP (Figure 6).

The cumulative effect of all of the changes during the **E_m-S** → **E_b-S** transition is an enhancement by 18.0 kcal/mol in the substrate binding energy (Table 1). The electrostatic contribution to the binding energy has also significantly increased (by 51.4 kcal/mol). Importantly, in the **E_b-S** complex, the binding energy of the α site for a metal is strongly enhanced when compared to the mononuclear complex (by 89.0 kcal/mol), whereas the β site also displays a strong affinity for a metal (Table 2), in good agreement with experimental data.[13,32]

Table 2. Comparison between Binding Energies of Both (α) and (β) Metals per Complex[a]

complex	ΔE_{vdW}	ΔE_{elec}	ΔG_{polar}	$\Delta G_{nonpolar}$	$\Delta G_{binding}$
$E_{m\alpha}$	19.2	−320.3	228.9	−0.8	−73.0 ± 12.5
E_m-S_α	18.9	−353.8	242.7	−0.8	−93.0 ± 4.6
E_b-S_α	31.9	−537.1	324.1	−0.9	−182.0 ± 6.9
E_b-S_β	28.6	−526.3	306.3	−0.8	−192.2 ± 5.4
$E_{b\alpha}$	25.3	−495.2	337.3	−0.9	−133.5 ± 3.4
$E_{b\beta}$	34.2	−521.2	314.3	−0.8	−173.5 ± 7.4
E_b-S_α^H	15.5	−329.4	238.6	−0.8	−76.2 ± 3.5
E_b-S_β^H	23.2	−379.7	240.8	−0.8	−116.6 ± 3.3
E_b-$S_{H81\text{-}A\text{-}\alpha}$	30.3	−531.4	320.9	−0.8	−181.0 ± 6.0
E_b-$S_{H81\text{-}A\text{-}\beta}$	26.4	−517.7	299.8	−0.9	−192.4 ± 7.0
E_b-$S_{H217\text{-}A\text{-}\alpha}$	30.4	−524.7	314.8	−0.9	−180.4 ± 7.9
E_b-$S_{H217\text{-}A\text{-}\beta}$	27.6	−516.0	302.5	−0.8	−186.7 ± 6.2
E_b-$S_{N80\text{-}A\text{-}\alpha}$	31.9	−519.0	322.2	−0.8	−165.7 ± 7.0
E_b-$S_{N80\text{-}A\text{-}\beta}$	20.7	−451.4	307.6	−0.9	−124.0 ± 15.1

[a]The energies are in kilocalories per mole.

3.3.1. Effect of the Substrate on the Structure of the E_b-S Complex. To study the effect of the addition of the substrate b*p*NPP, a simulation was run on the **E_b-S** species, where the substrate was removed from the active site. The resulting structure (E_b in Figure 8) was compared to the fully active substrate-bound complex (**E_b-S** in Figure 6). There are a few notable differences. First, the Zn−Zn distance is elongated in the absence of the substrate by 0.13 Å (3.27 Å), moving closer to the distance obtained from the crystal structure (3.68 Å). Additionally, two terminal water molecules coordinate to the metals, thus replacing the substrate, whereas μ-OH remains in the same position in both complexes. Of particular interest is the observation that in the absence of the substrate, the bond between residue Asn80 and the metal in the β site is shortened by 0.13 Å, which is in support of this residue experimentally observed coordination flexibility (see above).[13,18] The opposite movement is observed for His10 and His195, where the addition of the substrate leads to a contraction of their bond distances to the metals in the α and β sites, respectively, by 0.16 Å. However, the contact map generated for this complex did not differ greatly from the fully active form (Figure 4d).

Importantly, and again in good agreement with experimental data, in the absence of the substrate, the binding energies for both metals are significantly decreased (by 48.5 and 18.7 kcal/mol for the α and β sites, respectively; Table 2).[32] These results indicate that the substrate helps to stabilize several primary residues within the active site as well as the catalytically active metals, but they also demonstrate that once formed, the bimetallic center does not dissociate easily in the absence of the substrate. This interpretation thus agrees with kinetic measurements using both stopped-flow[13] and nuclear magnetic resonance[58] that showed that GpdQ employs a nonprocessive mechanism, whereby the active site remains assembled until the substrate is depleted.

3.3.2. Effect of the Bridging Hydroxyl Group on the Structure of the E_b-S Complex. The hydroxyl group that bridges the metals bound to the α and β sites has been proposed to function as a nucleophile in some binuclear metallohydrolases (e.g., some PAPs,[58,59] organophosphate-degrading hydrolases,[58,60,61] and antibiotic-degrading metallo-β-lactamases[58,62]), but in GpdQ, it was proposed to act as a base, abstracting a proton from a water bound to the metal in the α site, thus activating this water for its nucleophilic attack on the substrate.[13,18] To study its effect on the structure of the **E_b-S** complex, MD simulations were performed on a structure (**E_b-S^{-H}**) without this group. In this complex, the metal−metal distance is substantially longer than that in **E_b-S** (3.13 Å vs 4.74 Å; Figure 9) [RI (11,12) in Figure 4c and RI (10,11) in Figure 4e]. Additionally, a terminal water that is not observed in **E_b-S** coordinates to the metal in the α site in **E_b-S^{-H}**, and the first coordination shell Asp8 changes its coordination mode from mono- to μ-1,3 bidentate, effectively occupying the bridging position previously held by the μ-hydroxyl group [compare RI (1,11) in Figure 4e and RI (1,12) in Figure 4c]. This significant rearrangement of Asp8 was possibly due to the absence of a steric clash with that bridging hydroxyl group. The effect of the removal of μ-OH on the bond between Asn80 and the metal in the β site (1.90 Å) is comparable to that observed upon removing the substrate, demonstrating the synergistic nature of the substrate and metal bindings in the active site of GpdQ. Furthermore, in comparison to that in **E_b-S**, the bonds between b*p*NPP and the two metals in **E_b-S^{-H}** are more symmetric and tight (relevant bond length pairs are 1.78 Å/1.83 Å and 2.06 Å/1.87 Å for **E_b-S^{-H}** and **E_b-S**, respectively; Figures 6 and 9). This symmetry also translates into a higher substrate binding energy for **E_b-S^{-H}** (Table 1). In contrast, the binding energies for both metals in the absence of the μ-hydroxyl group (−76.2 and −116.6 kcal/mol for the metals in the α and β sites, respectively) are strongly reduced (Table 2), even though their respective coordination numbers (five and six) is unaltered.

The combined results observed upon removing the metal-bridging hydroxyl group thus demonstrate the relevance of this group in the formation of a stable bimetallic, catalytically active site. Its strong interaction with the two metals is anticipated to raise its alkaline character, thus enhancing its efficiency to activate the α-metal-bound nucleophile. Furthermore, the

DOI: 10.1021/acs.jpcb.8b02046
J. Phys. Chem. B 2018, 122, 5797−5808

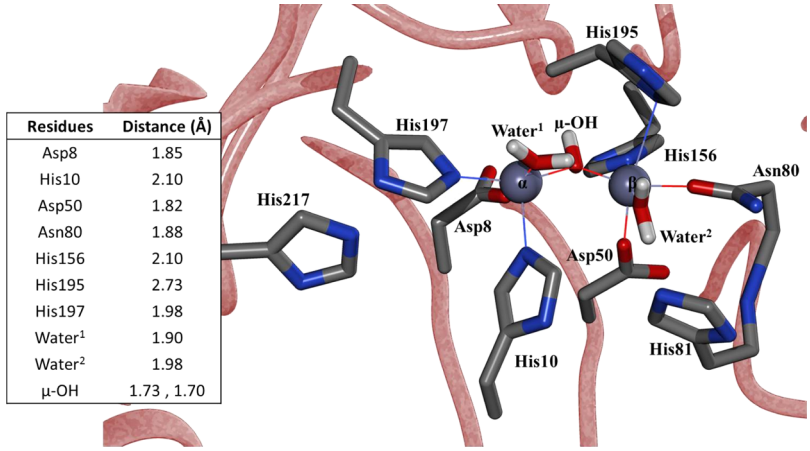

Residues	Distance (Å)
Asp8	1.85
His10	2.10
Asp50	1.82
Asn80	1.88
His156	2.10
His195	2.73
His197	1.98
Water¹	1.90
Water²	1.98
μ-OH	1.73 , 1.70

Figure 8. Most representative structure of the substrate-free form (E_b) of E_b-S derived from MD simulations. The (α) and (β) metals are shown in purple and the coordinating distances are provided in the table.

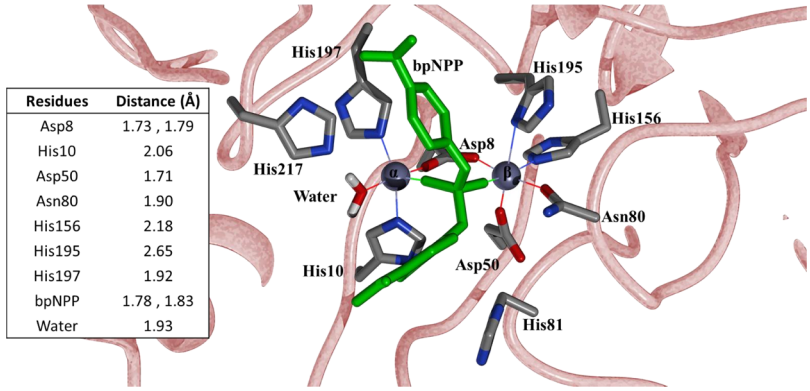

Residues	Distance (Å)
Asp8	1.73 , 1.79
His10	2.06
Asp50	1.71
Asn80	1.90
His156	2.18
His195	2.65
His197	1.92
bpNPP	1.78 , 1.83
Water	1.93

Figure 9. Most representative structure of the nucleophile (−OH) free form (E_b-S^{-H}) of E_b-S derived from MD simulations. The (α) and (β) metals are shown in purple, whereas the substrate b*p*NPP in green. The coordinating distances are provided in the table.

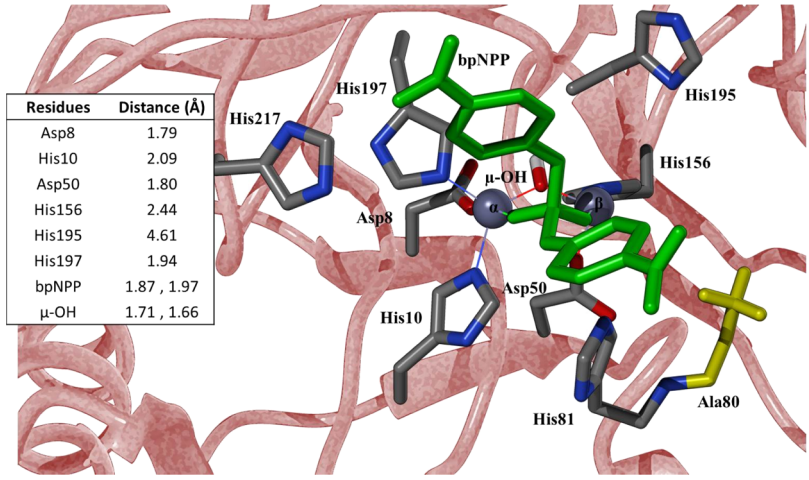

Residues	Distance (Å)
Asp8	1.79
His10	2.09
Asp50	1.80
His156	2.44
His195	4.61
His197	1.94
bpNPP	1.87 , 1.97
μ-OH	1.71 , 1.66

Figure 10. Most representative structure of the Asn80Ala mutant (E_b-S_{N80A}) of E_b-S derived from MD simulations. The (α) and (β) metals are shown in purple, the substrate b*p*NPP in green, and the mutation is in yellow. The coordinating distances are provided in the table.

presence of μ-OH also renders the enzyme−substrate complex more labile, thus lowering the activation barrier of the reaction.

3.3.3. Effects of Mutations on the Structure of the E_b-S Complex. The effects of three key residues (Asn80, His81, and His217) on the structure of the E_b-S complex were investigated next using their mutant forms (i.e., Asn80Ala, His81Ala, and His217Ala). Asn80 was shown experimentally to play an important role in both substrate and metal bindings,[33] and our computational data support this conclusion (vide supra). This residue directly coordinates to the metal in the β site and acts as a gate to block its exit. It also positions the substrate at the active site through hydrogen bonding. The Asn80Ala mutant of GpdQ, while shown to be catalytically active,[18] is thus expected to have decreased affinities for both the substrate and the metal

DOI: 10.1021/acs.jpcb.8b02046
J. Phys. Chem. B 2018, 122, 5797−5808

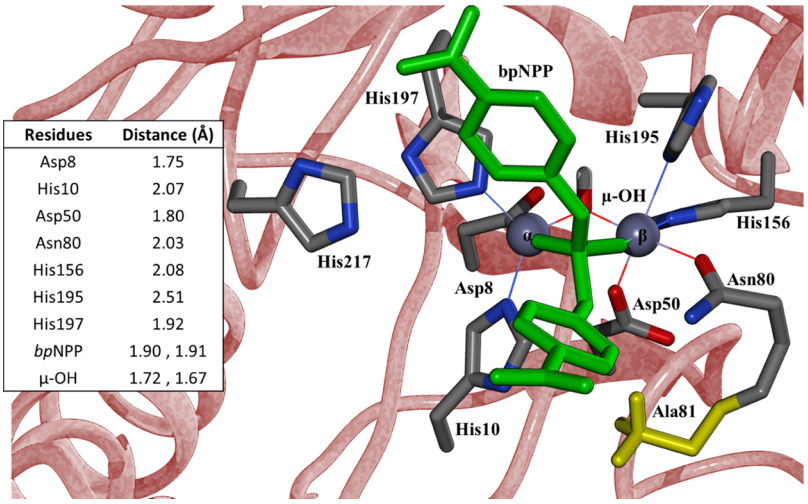

Figure 11. Most representative structure of the His81Ala mutant ($\mathbf{E_b}$-$\mathbf{S_{H81A}}$) of $\mathbf{E_b}$-**S** derived from MD simulations. The (α) and (β) metals are shown in purple, the substrate b*p*NPP in green, and the mutation is in yellow. The coordinating distances are provided in the table.

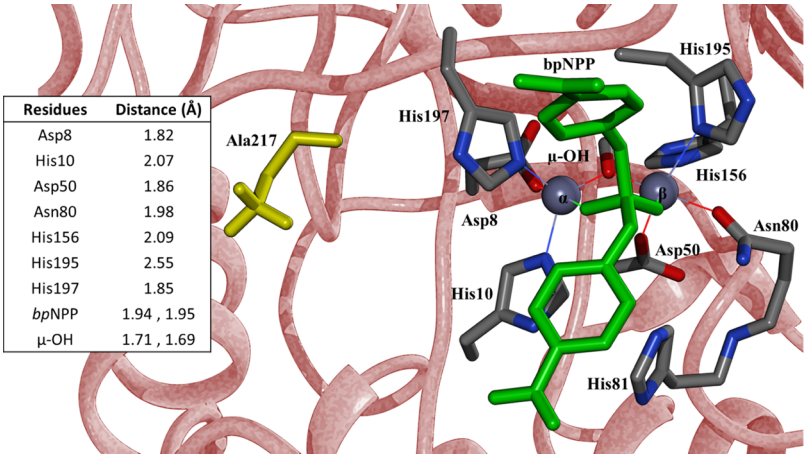

Figure 12. Most representative structure of the His217Ala mutant ($\mathbf{E_b}$-$\mathbf{S_{H217A}}$) of $\mathbf{E_b}$-**S** derived from MD simulations. The (α) and (β) metals are shown in purple, the substrate b*p*NPP in green, and the mutation is in yellow. The coordinating distances are provided in the table.

in the β site. In the structure derived from the MD simulation of this mutant ($\mathbf{E_b}$-$\mathbf{S_{N80A}}$), substantial alterations in the active site configuration are observed (Figure 10). The β metal binding site collapsed, and the coordination bond between the metal in this site and His195 is broken (Figures 4h and 10). In addition, greater fluctuations are observed for the metal in this site when compared to $\mathbf{E_b}$-**S** (Figure 4c,h) as it has more space to move. It is thus not surprising (and in agreement with experimental data[18]) that the substrate binding energy is reduced by 3.6 kcal/mol in this mutant. Furthermore, this mutation has a major impact on the binding energy of the metal in the β site (a reduction of nearly 70 kcal/mol), whereas the effect on the metal in the α site is moderate (Table 2). The computational data are thus in qualitative agreement with the available experimental data and demonstrate that a catalytically active bimetallic center can be maintained in GpdQ, even after a ligand of one of the metals is removed. This lends credence to the coordination flexibility of Asn80, initially proposed based on mutagenesis and spectroscopic data.[18]

The two second coordination shell residues His81 and His217 are part of an extensive hydrogen bond network that links the substrate binding pocket to the bimetallic catalytic center. Their replacement with Ala has a little effect on the catalytic efficiency of the resulting mutants; because the respective K_m values are also not altered largely by these mutations, it appears that these residues are not crucial for substrate binding.[13] However, an enhanced affinity in particular for the metal in the β site is observed, especially in the absence of the substrate.[13] In the most equilibrated calculated structure ($\mathbf{E_b}$-$\mathbf{S_{H81A}}$) derived from the simulation of the His81Ala mutant, the interaction between the residue in position 81 and the substrate is broken and the side chain is moved away from the binuclear metal center (Figure 11). However, the overall configuration of the active site is not greatly affected by this mutation (Figure 4f); the rmsd value obtained from a superposition of this and the crystal structure is low (0.40 Å). In agreement with the experimental data, the substrate binding energy in this mutant is very similar (slightly enhanced) to that of the wt enzyme (Table 1). Furthermore, the metal affinity for both binding sites is virtually identical to that of $\mathbf{E_b}$-**S** (Table 2). The mutation of His217 to Ala produced similar effects and active site coordination compared to the His81Ala mutant as shown by the contact maps (Figure 4f,g). In this case, the binding energy shows an increase of 3.1 kcal/mol. The equilibrated structure ($\mathbf{E_b}$-$\mathbf{S_{H217A}}$) obtained from this simulation is shown in Figure 12. The electrostatic energy

DOI: 10.1021/acs.jpcb.8b02046
J. Phys. Chem. B 2018, 122, 5797−5808

contribution for both mutants shows a minor increase and may be attributed to a slight decrease in the size of the binding pocket. It is also apparent that interactions that were lost due to mutation of these two residues are largely compensated by other residues in the proximity of the active site. The mutation of His81 to Ala enables the amine group of the primary shell residue Asn80 to form a hydrogen bond with the substrate at a distance of 1.94 Å. The His217 to Ala mutation allows for Tyr19 to move closer to the substrate to form a Π−Π interaction with the aromatic group of b*p*NPP at a distance of 3.36 Å.

Thus, while some outcomes of the calculations (in particular the break of the bond between His195 and the metal in the β site in the Asn80Ala mutant of GpdQ) contrast experimental data, the two approaches largely agree with respect to the role of the mutated residues in the catalytic mechanism.

4. SUMMARY AND CONCLUSIONS

GpdQ is an unusual metallohydrolase that requires the addition of a substrate in order to form a catalytically active binuclear metal center.[10,13,18] Furthermore, upon forming a bimetallic center, conformational changes in the active site alter the coordination environment of the metal in the β site (illustrated by the flexibility of ligand Asn80) and enhance the reactivity further. However, once formed, the catalytic center remains assembled until the substrate is depleted.[13,58] Because GpdQ is a promising agent for applications in agricultural bioremediation and the decontamination of nerve agents, understanding the details of its highly regulated mechanism is necessary to optimize its properties for specific applications.[14] The purpose of this study was the development of a computational methodology to probe this mechanism with a view to designing specific modifications (mutations) that may lead to desired alterations of the enzyme's catalytic properties (e.g., improving its catalytic rate and enhancing its stability). In our MD simulations, we focused on the initial stage of the catalytic cycle, i.e., the transformation of a catalytically inactive mononuclear form to a fully active bimetallic one. We considered the role of the substrate in this transition, as well as that of the proposed nucleophile of the reaction, i.e., the metal-bridging hydroxide group. Overall, we observed a good agreement between the simulated processes and those proposed based on experimental data.

In the resting state, the inactive mononuclear system ($\mathbf{E_m}$) has a Zn(II) bound to the α site; the metal-free β site is rather exposed to the solvent in an open conformation (Figure 3). The coordination of the substrate b*p*NPP to the metal ion of $\mathbf{E_m}$ significantly alters the active site and generates the $\mathbf{E_m}$-**S** species (Figure 5). Furthermore, the addition of the substrate enhances the bonding interaction between the metal and all of its four amino acid ligands (i.e., Asp8, His10, Asp50, and His197). Importantly, substrate binding also induces a shift of the gating residue Asn80 further away from the α site, a move that is accompanied by a reorientation of its side chain to facilitate coordination with a metal in the β site. Thus, the addition of b*p*NPP effectively primes the active site for the formation of a catalytically essential bimetallic center. This observation is in excellent agreement with a stopped-flow fluorescence study that demonstrated that the initial association between $\mathbf{E_m}$ and a substrate molecule rapidly (~350 s^{-1}) leads to a primed complex that is capable of accommodating a second metal ion (thus leading to the formation of $\mathbf{E_b}$-**S** with a rate of ~40 s^{-1}; Figure 6).[13] In $\mathbf{E_b}$-**S**, b*p*NPP adopts a metal-bridging μ-1,3 coordination mode. Importantly, in the presence of the substrate, the affinity of the metal in the α site is significantly enhanced (the binding free energy doubles from ~−90 to ~−180 kcal/mol; Table 2), which follows the trend observed in calorimetric[32] and spectroscopic[13] measurements. Furthermore, the β site also has a high affinity for a metal ion. The calculated metal affinity of the β site is ~10 kcal/mol greater than that of the α site. Although this observation contrast the relative binding affinities of the two sites determined by calorimetric methods, it should be noted that the calculations were carried out with Zn(II), whereas the experimental data were obtained for the Co(II) and Mn(II) derivatives of GpdQ. Although for both of these metals, the α site does display a higher affinity than the β site, this difference is far more pronounced in the Co(II) derivative. Thus, the relative affinities of the two metal binding sites may depend on the identity of the metals, but the affinity-enhancing effect of the substrate is ubiquitous. Insofar, the calculated affinities of the Zn(II) derivative of GpdQ are consistent with experimental values.

It is known from kinetic measurements that the transition of the catalytically noncompetent $\mathbf{E_m}$-**S** complex to the fully active $\mathbf{E_b}$-**S** complex takes approximately 25 ms.[13] Additional kinetic measurements demonstrated that it takes another ~1 min before GpdQ reaches its optimal catalytic efficiency. This lag period was shown to be associated with the flexibility of residue Asn80 in the β site. Thus, once formed the bimetallic center is not expected to disintegrate until the substrate is depleted. Indeed, our calculations reveal that while the removal of the substrate from $\mathbf{E_b}$-**S** (see Figure 8) has a negative impact on the affinities of both metals, the effect is too small to lead to a dissociation of these metals (Table 2).

The calculations also support the role of the metal-bridging hydroxide as the activator of the hydrolysis-initiating nucleophile. In silico, removal of this μ-OH group leads to a significant expansion of the metal−metal distance and the formation of a more symmetric enzyme−substrate complex (Figure 9). These observations indicate that μ-hydroxide interacts strongly with both metals, a process that greatly enhances its basic character and thus its ability to act as an efficient promoter of the hydrolytic reaction. Furthermore, by imposing a less symmetric and hence more strained conformation on the enzyme−substrate complex, a reduction of the activation barrier is achieved.

The calculations also successfully demonstrated the importance of residues Asn80, His81, and His217 in the mechanism of GpdQ. Some discrepancies, however, between experimental and theoretical studies ought to be noted. The calculations have not reproduced the full coordination flexibility of Asn80, a process that is relevant for the enzyme to obtain its catalytically most efficient conformation.[13] Nonetheless, we did observe an elongation of the bond between the metal in the β site and this ligand when the substrate is added (compare complexes $\mathbf{E_b}$ and $\mathbf{E_b}$-**S**). It is likely that the discrepancy between the experimental and theoretical extent of flexibility at this site is linked to the position of residue Asp50. According to the crystal structure, this aspartate bridges the two metal ions in $\mathbf{E_b}$-**S**. However, in the calculated structure, Asp50 is monodentately coordinated to the metal in the β site only. The switch of Asp50 from a coordinating position of the α metal to the β metal is likely to be consistent with data derived in a spectroscopic study with the Asn80Asp mutant of GpdQ.[13] In that study, the loss of enzymatic activity of the mutant was

DOI: 10.1021/acs.jpcb.8b02046
J. Phys. Chem. B 2018, 122, 5797−5808

ascribed to the reduced structural flexibility in position 80, leading to the breakage of one of the bonds between the bridging hydroxide moiety and its metal ligands. In a future study, our efforts will focus on factors that guide the movements of these residues. Nonetheless, the outcomes of our studies are encouraging as they provide the first theoretical approach to successfully recreate various aspects of a complex hydrolytic reaction carried out by an enzyme that employs an intricate regulatory mechanism of action.

■ ASSOCIATED CONTENT

Supporting Information

The Supporting Information is available free of charge on the ACS Publications website at DOI: 10.1021/acs.jpcb.8b02046.

RMSD of the Cα of the **Em**, **Em-S**, **Eb-S**, and **Em-S** trajectories plotted verse time and RMSD of the Cα of the **Eb-S-H**, **Eb-SN80A**, **Eb-SH81A**, and **Em-SH217A** trajectories plotted verse time (PDF)

■ AUTHOR INFORMATION

Corresponding Author

*E-mail: rpr@miami.edu. Phone: 305-284-9372. Fax: 305-284-4571.

ORCID

Rajeev Prabhakar: 0000-0003-1137-1272

Notes

The authors declare no competing financial interest.

■ ACKNOWLEDGMENTS

This material is based upon work supported by the grant from the National Science Foundation (grant number CHE-1664926) to R.P. Computational resources from the Center for Computational Science (CCS) at the University of Miami are greatly appreciated.

■ REFERENCES

(1) Nuttleman, P.; Roberts, M. Transfer of Iron from Uteroferrin (Purple Acid Phosphatase) to Transferrin Related to Acid Phosphatase Activity. *J. Biol. Chem.* **1990**, *265*, 12192−12199.

(2) Kaija, H.; Alatalo, S. L.; Halleen, J. M.; Lindqvist, Y.; Schneider, G.; Väänänen, H. K.; Vihko, P. Phosphatase and Oxygen Radical-Generating Activities of Mammalian Purple Acid Phosphatase Are Functionally Independent. *Biochem. Biophys. Res. Commun.* **2002**, *292*, 128−132.

(3) Räisänen, S. R.; Alatalo, S. L.; Ylipahkala, H.; Halleen, J. M.; Cassady, A. I.; Hume, D. A.; Väänänen, H. K. Macrophages Overexpressing Tartrate-Resistant Acid Phosphatase Show Altered Profile of Free Radical Production and Enhanced Capacity of Bacterial Killing. *Biochem. Biophys. Res. Commun.* **2005**, *331*, 120−126.

(4) Oddie, G. W.; Schenk, G.; Angel, N. Z.; Walsh, N.; Guddat, L. W.; de Jersey, J.; Cassady, A. I.; Hamilton, S. E.; Hume, D. A. Structure, Function, and Regulation of Tartrate-Resistant Acid Phosphatase. *Bone* **2000**, *27*, 575−584.

(5) Mitić, N.; Smith, S. J.; Neves, A.; Guddat, L. W.; Gahan, L. R.; Schenk, G. The Catalytic Mechanisms of Binuclear Metallohydrolases. *Chem. Rev.* **2006**, *106*, 3338−3363.

(6) Jackson, M. D.; Denu, J. M. Molecular Reactions of Protein Phosphatases Insights from Structure and Chemistry. *Chem. Rev.* **2001**, *101*, 2313−2340.

(7) Wilcox, D. E. Binuclear Metallohydrolases. *Chem. Rev.* **1996**, *96*, 2435−2458.

(8) Crowder, M. W.; Spencer, J.; Vila, A. J. Metallo-β-Lactamases: Novel Weaponry for Antibiotic Resistance in Bacteria. *Acc. Chem. Res.* **2006**, *39*, 721−728.

(9) Lowther, W. T.; Matthews, B. W. Metalloaminopeptidases: Common Functional Themes in Disparate Structural Surroundings. *Chem. Rev.* **2002**, *102*, 4581−4608.

(10) Daumann, L. J.; McCarthy, B. Y.; Hadler, K. S.; Murray, T. P.; Gahan, L. R.; Larrabee, J. A.; Ollis, D. L.; Schenk, G. Promiscuity Comes at a Price: Catalytic Versatility vs Efficiency in Different Metal Ion Derivatives of the Potential Bioremediator GpdQ. *Biochim. Biophys. Acta, Proteins Proteomics* **2013**, *1834*, 425−432.

(11) Gerlt, J. A.; Westheimer, F. H. Phosphodiesterase from Enterobacter Aerogenes. *J. Am. Chem. Soc.* **1973**, *95*, 8166−8168.

(12) Gerlt, J. A.; Whitman, G. J. Purification and Properties of a Phosphohydrolase from Enterobacter Aerogenes. *J. Biol. Chem.* **1975**, *250*, 5053−5058.

(13) Hadler, K. S.; Mitić, N.; Ely, F.; Hanson, G. R.; Gahan, L. R.; Larrabee, J. A.; Ollis, D. L.; Schenk, G. Structural Flexibility Enhances the Reactivity of the Bioremediator Glycerophosphodiesterase by Fine-Tuning Its Mechanism of Hydrolysis. *J. Am. Chem. Soc.* **2009**, *131*, 11900−11908.

(14) Schenk, G.; Mateen, I.; Ng, T.-K.; Pedroso, M. M.; Mitić, N.; Jafelicci, M.; Marques, R. F. C.; Gahan, L. R.; Ollis, D. L. Organophosphate-Degrading Metallohydrolases: Structure and Function of Potent Catalysts for Applications in Bioremediation. *Coord. Chem. Rev.* **2016**, *317*, 122−131.

(15) Ghanem, E.; Li, Y.; Xu, C.; Raushel, F. M. Characterization of a Phosphodiesterase Capable of Hydrolyzing EA 2192, the Most Toxic Degradation Product of the Nerve Agent VX. *Biochemistry* **2007**, *46*, 9032−9040.

(16) Ghanem, E.; Raushel, F. Detoxification of Organophosphate Nerve Agents by Bacterial Phosphotriesterase. *Toxicol. Appl. Pharmacol.* **2005**, *207*, 459−470.

(17) Daumann, L. J.; Larrabee, J. A.; Ollis, D.; Schenk, G.; Gahan, L. R. Immobilization of the Enzyme GpdQ on Magnetite Nanoparticles for Organophosphate Pesticide Bioremediation. *J. Inorg. Biochem.* **2014**, *131*, 1−7.

(18) Hadler, K. S.; Tanifum, E. A.; Yip, S. H.-C.; Mitić, N.; Guddat, L. W.; Jackson, C. J.; Gahan, L. R.; Nguyen, K.; Carr, P. D.; Ollis, D. L.; et al. Substrate-Promoted Formation of a Catalytically Competent Binuclear Center and Regulation of Reactivity in a Glycerophosphodiesterase from Enterobacter Aerogenes. *J. Am. Chem. Soc.* **2008**, *130*, 14129−14138.

(19) Selleck, C.; Clayton, D.; Gahan, L. R.; Mitić, N.; McGeary, R. P.; Pedroso, M. M.; Guddat, L. W.; Schenk, G. Visualization of the Reaction Trajectory and Transition State in a Hydrolytic Reaction Catalyzed by a Metalloenzyme. *Chem.—Eur. J.* **2017**, *23*, 4778−4781.

(20) Schenk, G.; Gahan, L. R.; Carrington, L. E.; Mitić, N.; Valizadeh, M.; Hamilton, S. E.; de Jersey, J.; Guddat, L. W. Phosphate Forms an Unusual Tripodal Complex with the Fe−Mn Center of Sweet Potato Purple Acid Phosphatase. *Proc. Natl. Acad. Sci. U.S.A.* **2005**, *102*, 273−278.

(21) Guddat, L. W.; McAlpine, A. S.; Hume, D.; Hamilton, S.; de Jersey, J.; Martin, J. L. Crystal Structure of Mammalian Purple Acid Phosphatase. *Structure* **1999**, *7*, 757−767.

(22) Klabunde, T.; Sträter, N.; Fröhlich, R.; Witzel, H.; Krebs, B. Mechanism of Fe(III) − Zn(II) Purple Acid Phosphatase Based on Crystal Structures. *J. Mol. Biol.* **1996**, *259*, 737−748.

(23) Lindqvist, Y.; Johansson, E.; Kaija, H.; Vihko, P.; Schneider, G. Three-Dimensional Structure of a Mammalian Purple Acid Phosphatase at 2.2 Å Resolution with a μ-(Hydr)Oxo Bridged Di-Iron Center. *J. Mol. Biol.* **1999**, *291*, 135−147.

(24) Sträter, N.; Jasper, B.; Scholte, M.; Krebs, B.; Duff, A. P.; Langley, D. B.; Han, R.; Averill, B. A.; Freeman, H. C.; Guss, J. M. Crystal Structures of Recombinant Human Purple Acid Phosphatase with and without an Inhibitory Conformation of the Repression Loop. *J. Mol. Biol.* **2005**, *351*, 233−246.

(25) Schenk, G.; Elliott, T. W.; Leung, E.; Carrington, L. E.; Mitić, N.; Gahan, L. R.; Guddat, L. W. Crystal Structures of a Purple Acid Phosphatase, Representing Different Steps of This Enzyme's Catalytic Cycle. *BMC Struct. Biol.* **2008**, *8*, 1−6.

DOI: 10.1021/acs.jpcb.8b02046
J. Phys. Chem. B 2018, 122, 5797−5808

(26) Hopfner, K.-P.; Karcher, A.; Craig, L.; Woo, T. T.; Carney, J. P.; Tainer, J. A. Structural Biochemistry and Interaction Architecture of the DNA Double-Strand Break Repair Mre11 Nuclease and Rad50-Atpase. *Cell* **2001**, *105*, 473−485.
(27) Lowther, W. T.; Matthews, B. W. Structure and Function of the Methionine Aminopeptidases. *Biochim. Biophys. Acta, Protein Struct. Mol. Enzymol.* **2000**, *1477*, 157−167.
(28) Mitić, N.; Miraula, M.; Selleck, C.; Hadler, K. S.; Uribe, E.; Pedroso, M. M.; Schenk, G. Catalytic Mechanisms of Metallohydrolases Containing Two Metal Ions. In *Advances in Protein Chemistry and Structural Biology*; Christov, C. Z., Ed.; Academic Press, 2014; Chapter 3, Vol. *97*, pp 49−81.
(29) Pedroso, M. M.; Larrabee, J. A.; Ely, F.; Gwee, S. E.; Mitić, N.; Ollis, D. L.; Gahan, L. R.; Schenk, G. Ca^{II} Binding Regulates and Dominates the Reactivity of a Transition-Metal-Ion-Dependent Diesterase from Mycobacterium Tuberculosis. *Chem.—Eur. J.* **2016**, *22*, 999−1009.
(30) Jackson, C. J.; Carr, P. D.; Liu, J.-W.; Watt, S. J.; Beck, J. L.; Ollis, D. L. The Structure and Function of a Novel Glycerophosphodiesterase from Enterobacter Aerogenes. *J. Mol. Biol.* **2007**, *367*, 1047−1062.
(31) Mirams, R. E.; Smith, S. J.; Hadler, K. S.; Ollis, D. L.; Schenk, G.; Gahan, L. R. Cadmium(II) Complexes of the Glycerophosphodiester-Degrading Enzyme GpdQ and a Biomimetic N, O Ligand. *J. Biol. Inorg Chem.* **2008**, *13*, 1065−1072.
(32) Pedroso, M. M.; Ely, F.; Carpenter, M. C.; Mitić, N.; Gahan, L. R.; Ollis, D. L.; Wilcox, D. E.; Schenk, G. Mechanistic Insight from Calorimetric Measurements of the Assembly of the Binuclear Metal Active Site of Glycerophosphodiesterase (GpdQ) from Enterobacter Aerogenes. *Biochemistry* **2017**, *56*, 3328−3336.
(33) Hadler, K. S.; Mitić, N.; Yip, S. H.-C.; Gahan, L. R.; Ollis, D. L.; Schenk, G.; Larrabee, J. A. Electronic Structure Analysis of the Dinuclear Metal Center in the Bioremediator Glycerophosphodiesterase (GpdQ) from Enterobacter Aerogenes. *Inorg. Chem.* **2010**, *49*, 2727−2734.
(34) Schenk, G.; Neidig, M. L.; Zhou, J.; Holman, T. R.; Solomon, E. I. Spectroscopic Characterization of Soybean Lipoxygenase-1 Mutants: The Role of Second Coordination Sphere Residues in the Regulation of Enzyme Activity. *Biochemistry* **2003**, *42*, 7294−7302.
(35) Neidig, M. L.; Wecksler, A. T.; Schenk, G.; Holman, T. R.; Solomon, E. I. Kinetic and Spectroscopic Studies of N694c Lipoxygenase: A Probe of the Substrate Activation Mechanism of a Nonheme Ferric Enzyme. *J. Am. Chem. Soc.* **2007**, *129*, 7531−7537.
(36) Becke, A. D. Density-Functional Thermochemistry. III. The Role of Exact Exchange. *J. Chem. Phys.* **1993**, *98*, 5648−5652.
(37) Francl, M. M.; Pietro, W. J.; Hehre, W. J.; Binkley, J. S.; Gordon, M. S.; DeFrees, D. J.; Pople, J. A. Self-Consistent Molecular Orbital Methods. XXIII. A Polarization-Type Basis Set for Second-Row Elements. *J. Chem. Phys.* **1982**, *77*, 3654−3665.
(38) Frisch, M. J.; Trucks, G. W.; Schlegel, H. B.; Scuseria, G. E.; Robb, M. A.; Cheeseman, J. R.; Scalmani, G.; Barone, V.; Mennucci, B.; Petersson, G. A.; et al. *Gaussian 09*; Gaussian, Inc.: Wallingford, CT, USA, 2009.
(39) Wang, J.; Wang, W.; Kollman, P. A.; Case, D. A. Automatic Atom Type and Bond Type Perception in Molecular Mechanical Calculations. *J. Mol. Graphics Modell.* **2006**, *25*, 247−260.
(40) Wang, J.; Wolf, R. M.; Caldwell, J. W.; Kollman, P. A.; Case, D. A. Development and Testing of a General AMBER Force Field. *J. Comput. Chem.* **2004**, *25*, 1157−1174.
(41) Case, D. A.; Betz, R. M.; Botello-Smith, W.; Cerutti, D. S.; Cheatham, T. E.; Darden, T. A.; Duke, R. E.; Giese, T. J.; Gohlke, H.; Goetz, A. W.; et al. *AMBER*; University of California: San Francisco, 2016.
(42) Trott, O.; Olson, A. J. Autodock Vina: Improving the Speed and Accuracy of Docking with a New Scoring Function, Efficient Optimization and Multithreading. *J. Comput. Chem.* **2010**, *31*, 455−461.
(43) Oostenbrink, C.; Villa, A.; Mark, A. E.; Van Gunsteren, W. F. A Biomolecular Force Field Based on the Free Enthalpy of Hydration and Solvation: The Gromos Force-Field Parameter Sets 53a5 and 53a6. *J. Comput. Chem.* **2004**, *25*, 1656−1676.
(44) Lindahl, E.; Hess, B.; van der Spoel, D. Gromacs 3.0: A Package for Molecular Simulation and Trajectory Analysis. *J. Mol. Model.* **2001**, *7*, 306−317.
(45) Case, D. A.; Cheatham, T. E.; Darden, T.; Gohlke, H.; Luo, R.; Merz, K. M.; Onufriev, A.; Simmerling, C.; Wang, B.; Woods, R. J. The AMBER Biomolecular Simulation Programs. *J. Comput. Chem.* **2005**, *26*, 1668−1688.
(46) Jorgensen, W. L.; Chandrasekhar, J.; Madura, J. D.; Impey, R. W.; Klein, M. L. Comparison of Simple Potential Functions for Simulating Liquid Water. *J. Chem. Phys.* **1983**, *79*, 926−935.
(47) Miyamoto, S.; Kollman, P. A. Settle: an Analytical Version of the Shake and Rattle Algorithm for Rigid Water Models. *J. Comput. Chem.* **1992**, *13*, 952−962.
(48) Hess, B.; Bekker, H.; Berendsen, H. J. C.; Fraaije, J. G. E. M. Lincs: A Linear Constraint Solver for Molecular Simulations. *J. Comput. Chem.* **1997**, *18*, 1463−1472.
(49) Darden, T.; York, D.; Pedersen, L. Particle Mesh Ewald: An N Log(N) Method for Ewald Sums in Large Systems. *J. Chem. Phys.* **1993**, *98*, 10089−10092.
(50) Pronk, S.; Páll, S.; Schulz, R.; Larsson, P.; Bjelkmar, P.; Apostolov, R.; Shirts, M. R.; Smith, J. C.; Kasson, P. M.; van der Spoel, D.; et al. Gromacs 4.5: A High-Throughput and Highly Parallel Open Source Molecular Simulation Toolkit. *Bioinformatics* **2013**, *29*, 845−854.
(51) Kumari, R.; Kumar, R.; Lynn, A. G_MMPBSA—a Gromacs Tool for High-Throughput MM-PBSA Calculations. *J. Chem. Inf. Model.* **2014**, *54*, 1951−1962.
(52) Homeyer, N.; Gohlke, H. Free Energy Calculations by the Molecular Mechanics Poisson−Boltzmann Surface Area Method. *Mol. Inf.* **2012**, *31*, 114−122.
(53) Joosten, R. P.; te Beek, T. A. H.; Krieger, E.; Hekkelman, M. L.; Hooft, R. W. W.; Schneider, R.; Sander, C.; Vriend, G. A Series of PDB Related Databases for Everyday Needs. *Nucleic Acids Res.* **2011**, *39*, D411−D419.
(54) Kabsch, W.; Sander, C. Dictionary of Protein Secondary Structure: Pattern Recognition of Hydrogen-Bonded and Geometrical Features. *Biopolymers* **1983**, *22*, 2577−2637.
(55) Krieger, E.; Vriend, G. Models@Home: Distributed Computing in Bioinformatics Using a Screensaver Based Approach. *Bioinformatics* **2002**, *18*, 315−318.
(56) Monsonego, A.; Zota, V.; Karni, A.; Krieger, J. I.; Bar-Or, A.; Bitan, G.; Budson, A. E.; Sperling, R.; Selkoe, D. J.; Weiner, H. L. Increased T Cell Reactivity to Amyloid β Protein in Older Humans and Patients with Alzheimer Disease. *J. Clin. Invest.* **2003**, *112*, 415−422.
(57) Pettersen, E. F.; Goddard, T. D.; Huang, C. C.; Couch, G. S.; Greenblatt, D. M.; Meng, E. C.; Ferrin, T. E. UCSF Chimera—a Visualization System for Exploratory Research and Analysis. *J. Comput. Chem.* **2004**, *25*, 1605−1612.
(58) Hadler, K. S.; Gahan, L. R.; Ollis, D. L.; Schenk, G. The Bioremediator Glycerophosphodiesterase Employs a Non-Processive Mechanism for Hydrolysis. *J. Inorg. Biochem.* **2010**, *104*, 211−213.
(59) Mitić, N.; Hadler, K. S.; Gahan, L. R.; Hengge, A. C.; Schenk, G. The Divalent Metal Ion in the Active Site of Uteroferrin Modulates Substrate Binding and Catalysis. *J. Am. Chem. Soc.* **2010**, *132*, 7049−7054.
(60) Aubert, S. D.; Li, Y.; Raushel, F. M. Mechanism for the Hydrolysis of Organophosphates by the Bacterial Phosphotriesterase. *Biochemistry* **2004**, *43*, 5707−5715.
(61) Ely, F.; Hadler, K. S.; Gahan, L. R.; Guddat, L. W.; Ollis, D. L.; Schenk, G. The Organophosphate-Degrading Enzyme from Agrobacterium Radiobacter Displays Mechanistic Flexibility for Catalysis. *Biochem. J.* **2010**, *432*, 565−573.
(62) Selleck, C.; Larrabee, J. A.; Harmer, J.; Guddat, L. W.; Mitić, N.; Helweh, W.; Ollis, D. L.; Craig, W. R.; Tierney, D. L.; Pedroso, M. M.; et al. AIM-1: An Antibiotic-Degrading Metallohydrolase That Displays Mechanistic Flexibility. *Chem.—Eur. J.* **2016**, *22*, 17704−17714.

DOI: 10.1021/acs.jpcb.8b02046
J. Phys. Chem. B 2018, 122, 5797−5808